Cerebrospinal Fluid Efflux Through Dynamic Paracellular Pores on Venule as a Missing Piece for the Image of Brain Drainage System

Yaqiong Dong
Peking University Health Science Center
Ting Xu
Peking University Health Science Center
Lan Yuan
Peking University Health Science Center
Yahan Wang
Peking University Health Science Center
Siwang Yu
Peking University Health Science Center
Zhi Wang
Peking University Health Science Center
Weiguang Zhang
Peking University Health Science Center
Weijiang He
Peking University Health Science Center
Xiaoda Yang
xyang@bjmu.edu.cn

Peking University Health Science Centre https://orcid.org/0000-0003-2282-6594

Research article

Keywords: Dynamic asymmetric pores, perivascular space dilation, Aβ clearance, tight junctions (TJs), brain drainage pathway

Posted Date: October 11th, 2021

DOI: https://doi.org/10.21203/rs.3.rs-941995/v1

Version of Record: A version of this preprint was published at Exploration on November 27th, 2023. See the published version at https://doi.org/10.1002/EXP.20230029.

Abstract

Background: The glymphatic system has been considered to contribute to a larger portion of parenchyma waste clearance and related to pathogenesis of many neural degenerative diseases such as the Alzheimer's disease (AD). However, up to date, the key route for the efflux from perivascular spaces to the blood pool remains a mystery.

Methods: BBB-impermeable fluorescent lanthanide probes of different size were first applied as cerebrospinal fluid (CSF)/interstitial fluid (ISF) tracers to quantitatively clarify the relative importance of different pathways to drain CSF/ISF solutes. The *in vivo* dynamic flows of subarachnoid CSF labeled with fluorescein isothiocyanate-dextran (4 kDa) tracers along brain blood vessels were observed under a two-photon confocal laser scanning microscope.

Results: Three phasic process for the brain drainage was observed, in which the rapid efflux of ISF solutes with a time constant close to the CSF oscillation during sleep appeals for new routes from perivenuous spaces to the blood pool. Careful observation on the dynamic efflux *in vivo* revealed a novel drainage pathway in which CSF molecules converge into the bloodstream directly through dynamic trumpet-like pores (basolateral *f* 8 μm; apical *f* 2 μm) on the wall of brain venule in mice. Zn^{2+}, an inducer of reconstruction of the tight junctions (TJs) in vascular endothelial cells, could facilitate the brain clearance of macromolecular ISF solutes. Deficit clearance of Aβ through the asymmetric pores on venule potentially causing perivascular space dilation was observed on the AD model mice.

Conclusions: The novel asymmetric pore path through reconstruction of endothelial TJs on the wall of venule shall provide a key piece for ISF solutes to drainage from brain in very rapid pathway. The update image would help to understand the structure and the regulation of glymphatic clearance of brain metabolites such as Aβ in search for the solutions of neurodegenerative diseases.

Background

In the brain, high metabolic rate and exquisite sensitivity of neurons and glia to extracellular environment changes require fast clearance of interstitial fluid (ISF) solutes especially metabolic wastes by efflux in blood-brain barrier (BBB) and the cerebrospinal fluid (CSF) drainage systems [1]. Recently, the astroglial-mediated ISF bulk flow, known as the glymphatic system, has been suggested to contribute to a larger portion of brain wastes clearance, especially the macromolecules and larger-sized particles such as amyloid β (Aβ) and its soluble aggregates [1–5]. It is proposed that, primarily during sleep [4], the gaps between vascular endothelial cells and astroglial cells are open and form a unique system of perivascular channels, through which CSF enters and flushes through cerebral parenchyma. Then the ISF carrying all kinds of interstitial solutes [2–4] would be collected in the paravenous spaces that was assumed to connect with the subpial and/or subarachnoid spaces [6], where CSF is either drained through lymphatics associated with extracranial segments of the cranial nerves and the meningeal lymphatic vessels into cervical lymph nodes (CLNs) [7, 8], or absorbed into the dural venous sinuses *via* the arachnoid

granulations/villi [6, 9]; the interstitial solutes are expected to be taken out of the brain following the CSF drainage.

Yet, questions and controversies remained on the anatomical structure of the perivascular spaces and the drainage pathways [10]. For example, why is Aβ deposited in pericapillary and periarteriolar membranes but not in perivenular membranes [11]? Why did abrogation of meningeal lymphatic vessels due to impaired VEGF-C/D–VEGFR3 signaling [12] could reduce clearance of macromolecules but not affect brain CSF water drainage? How could the Aβ after injection in parenchyma reach in blood in half hour, too sooner than the appearance of CSF tracer in CLNs [13]? Are there any alternative routes for CSF/ISF carrying interstitial solutes to exit the brain and explain the questions above [2, 10, 14]?

In searching for new efflux routes between the perivascular spaces and the blood pool, we noted the following facts: (1) the CSF oscillation dynamics was shown to couple to the brain's electrical activity [15], which may be correlated with the process of glymphatic pathway that mostly active during sleep; (2) Zn^{2+}, ions of an essential trace element, present in high concentration in the brain, especially in some regions such as lateral amygdala, subiculum and hippocampus. The rapidly exchangeable Zn^{2+} may transiently reach even up to 600 μM [16–20]; In fact, during neuronal activity, Zn^{2+} may be released into the synaptic cleft, resulting in transient local Zn^{2+} concentrations of 100–300 μM [21]; (3) Zn^{2+} may promote sleep efficiency and increase non-rapid eye movement (NREM) sleep [22–24], a critical factor activating glymphatic system [4, 5]; (4) Zn^{2+} at concentrations of 200 μM or above can regulate the epithelial tight junction architecture, causing the formation of asymmetric pore path favoring efflux particularly for macromolecules [25]. Thence, we hypothesize that there may exist certain dynamic asymmetric paracellular pores on venule regulated by waves of the brain's electrical activity, which may lead the paravenous fluids directly into the venous blood flow.

In the present work, we report the observation of dynamic formation of an asymmetric trumpet-like pore (basolateral φ: 5.9 μm; apical φ: 1.7 μm) on the wall of brain venule in mice using two-photon laser scanning microscopic imaging system. Through these asymmetric pores, CSF/ISF molecules were observed to directly converge into the bloodstream. As expected, addition of Zn^{2+} in perivenous flow could significantly promote formation of the outflow pores and facilitate brain clearance of the interstitial macromolecular solutes. Moreover, in Alzheimer disease (AD) model mice, reduced capacity of Aβ-content CSF/ISF drainage through the asymmetric pore path were observed, supporting sufficient brain drainage contributes to the pathogenic dilation of perivascular space and Aβ accumulation in AD. The present study may provide one new key piece for the intact image of brain glymphatic clearance system.

Materials And Methods

Materials

Fluorescein isothiocyanate-dextran 4 kDa (FD4) and Tetramethylrhodamine–dextran70 KDa (TRITC70) were from Sigma Aldrich Tech Co. (USA). Eu_2O_3 (99.99%) and Diethylenetriaminepentaacetic acid (DTPA)

were from Sinopharm Chemical Reagent Corp. (China). Bovine serum albumin (BSA) was from Amresco Inc. (USA). Artificial Cerebrospinal Fluid (ACSF) was from Leagene Corp. (China). Phosphate buffer saline (PBS) was from Hyclone (USA). Dimethylsulfoxide (DMSO) was from Sigma Aldrich Tech Co. (USA). Other reagents were of analytical grade.

Animals

C57BL/6 mice (male, 6-8 weeks old, SPF grade) were purchased from Peking University Health Science Center. APPswe/PS1dE9 (APP/PS1) transgenic mice and littermate negative C57BL/6 mice (male, 13-18 months old, SPF grade) were purchased from Model Animal Research Center of Nanjing University.

The mice were maintained and handled with the approval of Institutional Review Board for Laboratory Animal Care (Approval No. LA2017093), and fed in a barrier environment in Department of Laboratory Animal Science, Peking University Health Science Center. The mice were group-housed in a 12-hour light/12-hour dark cycle with ad libitum access to food and water. All experiments were performed in the light phase of the light/dark cycle. Anesthesia before experiment was administered using pentobarbital sodium (1% in saline, 80 mg/kg, intraperitoneal injection). All efforts were made to keep animal usage to a minimum.

Preparation of Eu complexes and Zn^{2+} fluorescent sensor (NBD-TPEA)

All Eu complexes were prepared according to the previous method [26]. The stock solutions of 0.01M $EuCl_3$ (pH 3.0) was prepared by dissolving 0.2760 g Eu_2O_3 in 5 ml of 3 M HCl and diluting to 100 ml with double distilled H_2O.

Eu-DTPA. To a 0.01M DTPA solution in Hank's balanced salt (HBSS; pH 7.0), 0.01M $EuCl_3$ was added dropwisely until appearance of a white sediment. The solution was kept at room temperature for 15 min, centrifuged (3 min, 10000×g), and the supernatant (Eu-DTPA) was collected.

Eu-BSA. Briefly, the DTPA-BSA conjugates were prepared by adding 18 mg DTPAA dissolved in DMSO to BSA (50 mg) solution in 5 ml of 0.1 M phosphate buffer with vigorous stirring. The coupling reaction proceeded 3–4 h at room temperature to allow the reaction to complete. Then, 0.01M $EuCl_3$ was added dropwisely until appearance of a white sediment to form Eu-DTPA-BSA (Eu-BSA). After centrifugation (3 min, 10000×g), the supernatant (Eu-BSA) was collected and applied to a PD-10 desalting column (GE Health Care, USA) pre-balanced with HBSS (pH 7.0). The elute was concentrated by centrifugal ultrafiltration (Amicon Ultra-4). The amount of BSA was measured with an enhanced BCA protein assay kit. The bound Eu was measured by time-resolved fluorescence as described in the previous method (fluorescent parameter: $\lambda_{ex/em}$ = 340/616 nm; measurement window, 600–1000 μs) [26].

Zn^{2+} fluorescent sensor (NBD-TPEA). NBD-TPEA was synthesized according to the previous method [27]. The stock solutions of 5 mM NBD-TPEA was prepared by dissolving 13 mg NBD-TPEA in 524 μl of DMSO

and diluting to 4.17 ml with PBS. NBD-TPEA is a visible light excitable Zn^{2+} fluorescent probe based on the nitrobenzoxadiazole fluorophore. The probe has a good zinc ion selective enhancement effect, which can bind Zn^{2+} in a ratio of 1:1 and emit fluorescence at 534 nm with 488 nm excitation. With good stokes displacement and biocompatibility, it is suitable for the quantitative measurements of zinc ion concentration *in vivo* or *in vitro*.

Pharmacokinetics of intrastriate Eu-DTPA injection in brain

To determine the kinetics of Eu-DTPA probe in brain, C57BL/6 mice (*n*=5) were intrastriate injected with Eu-DTPA probe. Specifically, anesthetized mice were fixed in a stereotaxic frame and body temperature was kept at 37 °C with a temperature-controlled warming pad. A 33 GA needle was inserted *via* a small burr hole into the brain at the following coordinates: intrastriate injections (0.22 mm caudal, 2.5 mm lateral, 3.5 mm ventral to bregma) [2]. After needle insertion, 30 minutes was elapsed to allow the needle track to swell closed, avoiding fluorescent agents leaking from the hole where the needle was inserted into the brain. 1.0 μl of Eu-DTPA probe (dissolved in ACSF) was injected at a rate of 0.1 μl/min with a syringe pump (Harvard Apparatus). Then, 5 min, 15 min, 0.5 h, 1 h, 3 h, 6 h, 12 h, and 24 h after the administration, animals were immediately decapitated with the skull opened, the dura removed and the brain harvested. Then, the brains of mice were added to 5 times the mass of pre-chilled deionized water and homogenized with a bullet blender (Gene Company Limited, Hong Kong). The homogenates were centrifuged at 5,000×g for 15 min and the supernatant was collected. Meanwhile, sterile 0.9 % saline was also intrastriate injected into mice as background control. Then, Eu content was measured by time-resolved fluorescence as described in the previous method (fluorescent parameter: $\lambda_{ex/em}$ = 340/616 nm; measurement window, 600–1000 μs)[26] and normalized to percent of total injected amount of Eu-DTPA probe. Eu-DTPA clearance from the brain was compared by two-way ANOVA.

Intrastriate Eu-BSA injection followed by Zn^{2+} intervention

C57BL/6 mice (male, SPF grade) were prepared and allocated randomly into four groups with 6 mice for each group: (I) Control; (II) Zn^{2+} (0.25 mM) group; (III) Zn^{2+} (0.5 mM) group; (IV) Zn^{2+} (1 mM) group.

First, anesthetized mice were fixed in a stereotaxic frame and body temperature was kept at 37 °C with a temperature-controlled warming pad. A 30 GA needle was inserted into the cisterna magna, 2 μl of normal ACSF, 0.25 mM, 0.5 mM and 1 mM Zn^{2+} (dissolved in ACSF) were injected at a rate of 0.2 μl/min over 10 min with a syringe pump (Harvard Apparatus) in (I)-(IV) groups, respectively. Thirty minutes after Zn^{2+} injection, Eu-BSA (constituted in ACSF) was injected into intrastriate to cycle for 30 min. A 33 GA needle was inserted *via* a small burr hole into the brain at the following coordinates: intrastriate injections (0.22 mm caudal, 2.5 mm lateral, 3.5 mm ventral to bregma). After needle insertion, 30 minutes was elapsed to allow the needle track to swell closed. 1.0 μl of Eu-BSA was injected at a rate of 0.1 μl/min with a syringe pump (Harvard Apparatus) in all the four experimental groups.

After 30 minutes, mice were immediately decapitated, the urine and the blood was collected and the brain harvested and homogenized. Eu content was also measured by time-resolved fluorescence as described

in the previous method and normalized to percent of total injected amount of Eu-BSA probe. Eu-BSA clearance from the brain and accumulation in the urine was compared by two-way ANOVA.

Intracisternal FD4 or Zn $^{2+}$ (+FD4) or Zn^{2+} fluorescent sensor injection in healthy wide-type mice and in vivo **fluorescence imaging**

C57BL/6 mice (male, 6–8 weeks old, SPF grade, 6 mice for each experiment) as healthy wide-type (WT) mice were prepared and maintained. A craniotomy (2×2 mm in diameter) was made over the cortex of the anesthetized mice. The dura was left intact and the craniotomy was covered with ACSF and sealed with a glass coverslip. Then anesthetized mice were fixed in a stereotaxic frame and a 30 GA needle was inserted into the cisterna magna. 2 μl of FD4 tracer or Zn^{2+} (together with FD4) or Zn^{2+} fluorescent sensor (NBD-TPEA), respectively, was injected at a rate of 0.2 μl/min over 10 min with a syringe pump (Harvard Apparatus). To visualize the cerebral vasculature, 0.1ml BBB impermeable Tetramethylrhodamine–dextran70 KDa (TRITC70) (MW 70kD, 1% in saline) was immediately injected intravenously before imaging.

After intracisternal injection of fluorescence tracers, tracer movement into the cortex was recorded with a confocal laser scanning microscope (Leica microsystems CMS GmbH D-35578 Wetzlar (DFC360 FX), Germany) with FITC-channel (FD4 tracer) or $\lambda_{ex/em}$ = 488/534 nm (Zn^{2+} fluorescent sensor) 512×512 pixel image acquisition. The detailed experiment of *in vivo* two-photon imaging would be depicted next.

Intracisternal FD4 injection in AD mice model and in vivo **fluorescence imaging**

The APP/PS1 transgenic mice (male, 13–18 months old, SPF grade, *n*=4–6) and littermate negative C57BL/6 mice (male, 13-18 months old, SPF grade, *n*=4–6) were prepared. The APP/PS1 mice over-express the deltaexon 9 variant of presenilin 1 (PS1) in combination with the Swedish mutation of β-amyloid precursor (APP). The FD4 tracer brain clearance experiments in the mice were conducted according to the methods mentioned as in healthy WT mice above.

In vivo **two-photon laser scanning microscopy**

For *in vivo* imaging, a craniotomy (2×2 mm in diameter) was made over the cortex 1 mm lateral and 0.5 mm posterior to bregma [2]. The dura was left intact and the craniotomy was covered with ACSF and sealed with a glass coverslip. To visualize the vasculature, 0.1 ml of BBB impermeable TRITC70 (MW 70 kD,1% in saline) was introduced by intravenous injection immediately before imaging. An HCX APO L 20×/1.00 water immersion lens was used to image the cortex, from the surface to a depth of ~300 μm. Excitation wavelength was 920 nm for TRITC70 and FD4, and emission was collected at 500–550 nm for FD4 and 575–625 nm for TRITC70. The cerebral vasculature 512×512 pixel frames from the surface to a depth of 300 μm with 0.5 or 1 μm z-steps by two-photon laser scanning microscopy were acquired. After intracisternal injection of CSF tracer, tracer movement into the cortex was conducted with dual-channel (FITC and TRITC) 512×512 pixel image acquisition.

The pores on brain blood vessels

The cerebral vasculature was first observed using CCD dynamic imaging, the pores on venule were observed by two-photon scanning when CSF tracer directly entered the brain blood vessels from some special positions along paravenous spaces. Images of the pores were conducted at 0.2, 0.5, or 1 μm intervals, and the diameter along the depth from the basolateral to apical was measured, respectively.

Quantitative analysis of dynamic pores was measured of all the fields of the craniotomy (2×2 mm in diameter). Mean values were calculated from 4–6 venules per animal in each region of different experimental groups. In order to observe the dynamic conditions of pores on venule, the special vessels would be tracked to be repeatedly scanned with 0.5 or 1 μm z-steps at 1 minute intervals for the duration of the experiment.

Statistical analysis

Data were expressed as mean ± standard deviation (SD) or mean ± standard Error of the Mean (SEM). Differences between groups were analyzed by two-way analysis of variance (ANOVA) and $p<0.05$ was considered as statistically significant. Statistical analyses were carried out using Origin 8.0 or SPSS.

Results

Novel pore path on venule wall account for the rapid drainage of CSF-ISF solutes in brain

The kinetic process for brain drainage was analyzed using a BBB-impermeable small molecular fluorescence tracer, europium-DTPA (Eu^{3+}-DTPA), which is neither a substrate of the efflux transporters on BBB. After intrastriatal injection of Eu^{3+}-DTPA (Fig. 1A), the brain content of the fluorescent tracer was observed to decrease rapidly with time, indicating a three phasic process for the brain drainage (Fig. 1B): (1) a very rapid one with a < 5 min time constant (τ), contributing ~25% of the tracer clearance under the test conditions. According to the CSF oscillation time [15], we assumed this rapid outflow has a $\tau \sim 24$ s; (2) a fast drainage with a τ of 2.1 h, contributing ~44% of tracer removal; and (3) a slow drainage with a τ of 9.5 h for the rest CSF-ISF solute excretion (~31%).

Next, whether CSF-ISF flux directly drain into blood stream from certain pore path on venule wall was investigated by fluorescence microscopic imaging. The CSF-ISF flux was labeled by cisterna magna infusion of fluorescein isothiocyanate–dextran-4 (FD4, molecular size, 4 kD) and the routes and time course of subarachnoid CSF flux into the brain parenchyma were recorded in real time through a closed cranial window in anesthetized mice (Fig. 1C). It is observed that CSF flux entered from the subarachnoid compartment into brain parenchyma, then flowed along the paravenous spaces meanwhile drained directly into brain venule blood in mice of both healthy (Fig. 1D) and AD model (Fig. 1E). More intuitively seen in Supplementary Movie 1&2, FD4 tracers flow in the paravascular space, penetrate into vessel chamber and move in the blood along the inner side of vascular wall. It is notable that compared to healthy WT mice, abundant tracer clogs were observed in the lumen of blood vessels at the site of the pore path and nearby area in AD model mice (Fig. 1E, indicated by yellow triangle).

Overall, the observations above indicated a novel pore pathway on the venule wall for CSF-ISF solutes to excrete into blood apart from the known efflux pathways [1].

In vivo **imaging reveals dynamic formation of asymmetric trumpet-like pores on venule wall**

With labelling of cerebral vasculature by tetramethylrhodamine–dextran-70 (TRITC70, molecular size, 70 kD) and CSF-ISF flux by FD4, the structure of the pore path on venule was closely observed by two-photon laser scanning fluorescence microscopy. As shown in Fig. 2A, pores on the venule wall were observed under the background of the fast-flowing bloodstream (BS) (dark shadows in the veins) on a light-section plane image on a CSF-ISF flux entry area. Further light section with various depth on a typical pore revealed an asymmetric trumpet-like structure (Fig. 2A, B) with the dimension of 5.5 μm in depth, 5.9 μm for basolateral diameter of and 1.7 μm for apical diameter. This asymmetric pore path was observed in venules with vascular caliber of ~15–200 μm. The average size for basolateral diameter was calculated to be 4.9±1.8 μm (Fig. 2C); accordingly, the apical diameter of the pores is expected to be <2 μm in average.

Observation in a two-hour period revealed dynamic formation for the asymmetric pores. As shown in Fig. 2D & E, the pores in the upper white circle area disappeared after 60 min; while pores emerged in the lower white circle area in the time period of 35–75 min. This is consistent with our expectation according to ref.[25].

Based on all the results above, we proposed that CSF-ISF in paravenous space could rapidly pass through the asymmetric trumpet-like pores into blood stream in one-way direction driven by the hydrodynamic pressure difference between the static ISF and the flowing blood (Fig. 2F). The unidirectional flow and the smaller apical size of the pores than blood cells prevent occurrence of cerebral hemorrhage through these dynamic pores.

Zinc ions promote the formation of the above asymmetric pores and rapid discharge of macromolecule

Previously, high concentrations (>200 mM) of Zn^{2+} from basolateral side of the Madin-Darby canine kidney (MDCK) cell monolayer have been demonstrated to induce the reconstruction of endothelial tight junctions (TJs) to form asymmetric trumpet-like pores [25]. Considering the potential transient local high concentration of Zn^{2+} in brain especially during neuronal activity, we have speculated a role of Zn^{2+} in remodeling the TJs structure of vascular endothelial cells (VECs) to form the trumpet-like pores (Fig. 3A).

To test this hypothesis, we firstly observed the spatial distribution of Zn^{2+} during paravscular CSF tracer movement into the pores using a Zn^{2+} fluorescence sensor (NBD-TPEA) (Fig. 3B). The result (Fig. 3C, highlighted by rectangle marks) showed that Zn^{2+} ions were present in spots that primarily spread along the vascular walls. Secondly, we assessed the relative amount of dynamic pores on venule after Zn^{2+} (in combination with FD4 tracers) intracisternal injection. The results (Fig. 3D-F) showed that additional Zn^{2+}

(0.5 mM) could significantly increase the formation of asymmetric pores compared to control mice. Thirdly, we tested rate of discharge of brain interstitial macromolecular wastes upon Zn^{2+} treatment (Fig. 3G). The results (Fig. 3H-J) showed that all Zn^{2+}-treated groups (especially 0.5 mM Zn^{2+} group) significantly decreased amounts of Eu-BSA retain in the brain (Fig. 3H), increased the levels of Eu-BSA in peripheral blood (Fig. 3I), and increased urinal tracers secretion in the 0.5 mM Zn^{2+}-treated group (Fig. 3J). All the results above indicated that CSF Zn^{2+} in appropriate concentrations could potentially promote the formation of the asymmetric pores and rapid discharge of macromolecular metabolic wastes in brain.

Heavy Aβ burden over clearance capacity through the pore path may contribute to the perivenous space dilation in AD model mice.

The formation of Aβ plaques is one hallmark in AD pathologensis while Aβ accumulation comes from imbalance between production and clearance from early stages of AD [1]. A variety of systems have been suggested being involved in clearance of extracellular Aβ deposits in brain, i.e. the BBB, the glymphatic system and the meningeal lymphatic vessels [1]. We thus investigated the performance of Aβ clearance through the asymmetric pores in AD model mice (Fig. 4).

As shown in Fig. 4A, after intracisternal injection in the brain of AD mice, FD4 tracers gathers in the perivenous area alongside a multiple of blood vessels. It is noted that most of the bands of FD4 tracers around brain venules in AD mice are significantly wider than those in WT healthy mice. A closer look at the blood vessel and perivascular space (Fig. 4B & C) revealed that the paravascular FD4 tracers was rather seemingly flowing around the vascular wall in numbers of pools connected with each other. When further carefully observing on a selected pool using light section with a two-photon laser scanning microscope (Fig. 4D & E), we could see at least one dynamic pore on the vascular wall underneath. Next, observation on larger magnification in more area revealed that abundant pore path exist on the venule walls, surrounded by the CSF flow (Fig. 4F & G). Two points noticeable here are: (1) AD mice showed increased amounts of pores (by 60%) on venule than the WT mice (Fig. 4F). This is consistent with our previous observation that AD mice showed a slightly increased rate of brain Aβ clearance [13]; (2) the FD4 tracers did not disperse evenly in the fluid near the pore path (Fig. 4G), suggesting that CSF in the paravenous pools would be viscous due to high content of Aβ.

The high viscosity of Aβ-content CSF would be more clearly seen in the movie record (Fig. 4H and Supplementary Movie 3). Unlike in the healthy mice that the CSF flux carrying the FD4 tracers forms smooth streams into the blood through the asymmetric pores (Supplementary Movie 4), the CSF flux would rather be like squeezing into the blood vessel chamber (Fig. 4H). At certain casual times, as shown in Supplementary Movie 5–7, the CSF clouds could even stay in the blood vessel for tens of seconds possibly due to temporary break of blood flow, and soon were flushed away when the blood flow recovered. These results suggest that the asymmetric pore path may exhibit significantly reduced capacity to transport the viscous Aβ-content CSF. Therefore, despite of increased formation of the

dynamic asymmetric pores in transgenic AD model mice, too much brain Aβ burden over the drainage capacity would lead to accumulation of Aβ-content CSF and thus next perivascular space dilation.

Discussion

To clarify the relative importance of different pathways to drain CSF/ISF solutes, we tested the drainage process of a small molecular and BBB impermeable fluorescent lanthanide probe (Eu^{3+}-DTPA complexes). Unlike the organic optical indicators, the lanthanide probe is rather stable to metabolic degradation in CSF and is one of the most sensitive indicator by taking the advantage of time-resolved fluorescence spectroscopic measurements. The results (Fig. 1A & B) showed multiple pathways with three major rates. The medium rate ($\tau \sim 2.0$ h), contributing to close to a half of CSF/ISF solute secretion, is apparently in agreement with drainage through the dural assigned lymphatics [12]; The slow one ($\tau \sim 10$ h) may suggest existence of certain reservoir or pools in brain for temporarily keeping the wastes especially during day time when the glymphatics are not active, which is plausible for further investigation.

The rapid one ($\tau < 5$ min) contributing to about a quarter of CSF/ISF solute clearance is most interesting. We assume this rapid clearance may be related to the ~ 24 s CSF oscillation during sleep, and its percentage of the CSF/ISF solute clearance may be underestimated because the animals were not observed under whole course anaesthesia. Such rapid rate of clearance may suggest closer distance or/and more direct discharge to the blood. Then what would the drainage pathway be?

Accidentally, in observing the dynamic process of subarachnoid CSF influx into brain parenchyma, we observed that fluorescence CSF/ISF tracers directly entered the brain blood vessels from certain sites along paravenous spaces (Fig. 1C~E; Supplementary Movie 1&2) after cisterna magna infusion. In AD mice, it is more obvious that the tracer gathered in certain area of the paravascular spaces and injected into the venous blood from some points on venule wall (Fig. 1E and Fig. 4A). Therefore, we further tracked and magnified the sites where the fluorescent tracers inject in the blood. We successively observed dynamic formation of the asymmetric trumpet-like pores on venule (Fig. 2A~E). By light section with a two-photon laser scanning microscope, the 3D parameters of the pores were estimated (Fig. 2A&B). The conical shape and the dynamic fluid pressure difference between blood flow and ISF would produce a unilateral efflux of ISF (Fig. 2F). The vascular pulsation may facilitate the ISF efflux as the pulse of ISF injection into blood occasionally observed at some large pores in AD mice (Supplementary Movie 8). Nonetheless, the small apical diameter (< 2 μm) excludes the possibility of leakage of any blood cells into brain parenchyma in physiological state.

The facts that Zn^{2+} promotes the formation of the asymmetric pores (Fig. 3D~F) and efflux of macromolecular tracer (Fig. 3G-J) may suggest a tight linkage between opening of the pore path and the coupled electrophysiological, hemodynamic, and CSF oscillations in sleep [15]. The neuronal activity may cause release of pulsatile high concentration of Zn^{2+} [21] observed herein as fluorescent spots (Fig. 3C). The transient local high concentrations of Zn^{2+} could induce remodeling of TJs [25] in VECs, thus

stimulating the formation of the asymmetric pore path (Fig. 3A) that provide an exit for the following CSF wave to flush through and take the metabolic waste out. This is consistent with increase of NREM sleep, a critical factor active glymphatic system [4, 5], upon dietary zinc supplementary [22–24]. Moreover, the ~0.04-Hz pulsatile inflow of CSF coupled to hemodynamic could provide additional driver of fluid movement through perivascular spaces.

It is noted that in transgenic AD mice, the high viscosity of Aβ-content ISF caused significantly reduced capacity for the asymmetric pore path to transport wastes (Fig. 4H and Supplementary Movie 3). In the present case, Aβ accumulation and dilation in some perivenous space segment were observed (Fig. 4A). We speculated that the excess amount of Aβ would further be transported to the subpial-subarachnoid spaces. Once in the CSF circulation, Aβ may on one hand impair or even block the CSF water drainage pathways, causing perivascular space dilation especially in the upstream section of CSF inflow [11, 28, 29]; on the other hand, Aβ may enter the periarteriolar spaces and deposited in periarteriolar membranes [11] due to the interactions with the vascular smooth muscle cells (VSMCs) [30, 31]; for instance, VSMCs in brain blood vessels express the α7 nicotinic acetylcholine receptor (α7nAChR), which has high binding affinity for Aβ peptides and facilitates the selective accumulation of Aβ peptides in VSMCs [32].

Obviously, the pore path formation requires the viable function of VECs. Thus, activation of VECs is expected to improve the brain clearance while the pathological factors causing VECs damage would impair it. Recently, it is reported that people who had recovered from COVID-19, including those no longer reporting symptoms, exhibited significant cognitive deficits [33]. A network-based, multimodal omics analysis links SARS-CoV-2/COVID-19 infection to brain microvascular injury and neuroinflammation [34]; in fact, the S1 subunit of the spike protein was shown to cause damage of endothelial cells of micro-vessels [35]. Thus, we speculated that impaired brain waste clearance due to damage of VECs may play a role in the cognitive impairment like that in AD. Enhancement of the brain glymphatic function while promoting the VECs recovery by agents (such as epidermal growth factors, EGFs) may help to prevent the loss of cognition in COVID-19 patients.

Conclusions

In summary, we discovered a novel asymmetric pore path on the wall of venule for ISF solutes to drainage from brain in very rapid pathway, which may provide a key piece for the glymphatic system. The update picture based on current findings would be like below (Fig. 5): firstly, the neuronal activity mostly associated with sleep induces releasing of Zn^{2+} (and possibly other neurotransmitters) to induce formation of the dynamic asymmetric pore path towards the bloodstream. Then the following wave of CSF enter *via* the periarteriolar spaces and flush through brain parenchyma, taking the interstitial solutes including macromolecules and large particles to the perivenous spaces and drain directly into blood *via* the pore path described. Most metabolic wastes would be expected to sweep away in this way. Nonetheless, excessive amounts of ISF solutes would reach CSF cycling at the subpial-subarachnoid spaces, where the solutes would be either clean up by the dural lymphatic systems or back cycling in the brain until clear away or deposit in brain (both periarteriolar space and parenchyma). The retention of

toxic metabolic wastes such as Aβ would accelerate the pathogenesis and progression of a variety of brain diseases.

Abbreviations

Aβ
Amyloidβ
APP/PS1
APPswe/PS1dE9
BBB
Blood-brain barrier
CLNs
Cervical lymph nodes
CSF
Cerebrospinal fluid
FD4
Fluorescein isothiocyanate-dextran 4 kDa
ISF
Interstitial fluid
MDCK
Madin-Darby canine kidney
NREM
Non-rapid eye movement
TJs
tight junctions
TRITC70
Tetramethylrhodamine–dextran70 Kda
VECs
Vascular endothelial cells
VEGF-C/D
vascular endothelial growth factors-C/D
VEGFR3
Vascular endothelial growth factor receptor 3.

Declarations

Acknowledgements

We thank Dr. Zengqiang Yuan at the Academy of Military Medical Sciences for providing the 5×FAD transgenic model mice to help further validate the experiment conclusion.

Authors contributions

X.D.Y. and W.G.Z. was responsible for the conception and design of the study. Y.Q.D. planned and carried out the experiments, analyzed the data, generated the figures, and wrote the manuscript. X.D.Y. and W.G.Z reviewed and edited the manuscript. Y.Q.D., T.X., L.Y., Y.H.W. and Z.W. were involved in the brain drainage system studies. S.W.Y. helped with animal experiments. W.J.H. was involved in synthesis of zinc probe. All authors read and approved the final manuscript.

Funding

This work was supported by National Natural Science Foundation of China (#21571006, #21771010 and #81873769).

Availability of data and materials

All data generated or analyzed during this study are included in this published article (and its supplementary information files) and all raw data are available from the authors upon reasonable request.

Ethics approval and consent to participate

Animal husbandry, housing and all procedures were performed following protocols with the approval of Institutional Review Board for Laboratory Animal Care.

Competing interests

The authors declare no competing interests.

Supplementary material

Supplementary material is available online.

References

1. Tarasoff-Conway JM, Carare RO, Osorio RS, et al. Clearance systems in the brain-implications for Alzheimer disease. Nat Rev Neurol. 2015;11(8):457–70.
2. Iliff JJ, Wang MH, Liao YH, et al. A Paravascular Pathway Facilitates CSF Flow Through the Brain Parenchyma and the Clearance of Interstitial Solutes, Including Amyloid beta. Sci Transl Med.

2012;4(147):147ra111.

3. Kress BT, Iliff JJ, Xia MS, et al. Impairment of Paravascular Clearance Pathways in the Aging Brain. Ann Neurol. 2014;76(6):845–61.
4. Xie LL, Kang HY, Xu QW, et al. Sleep Drives Metabolite Clearance from the Adult Brain. Science. 2013;342(6156):373–7.
5. Nedergaard M, Goldman SA. Glymphatic failure as a final common pathway to dementia. Science. 2020;370:50–6.
6. Proulx ST. Cerebrospinal fluid outflow: a review of the historical and contemporary evidence for arachnoid villi, perineural routes, and dural lymphatics. Cell Mol Life Sci. 2021;78:2429–57.
7. Louveau A, Smirnov I, Keyes TJ, et al. Structural and functional features of central nervous system lymphatic vessels. Nature. 2015;523(7560):337–41.
8. Da Mesquita S, Louveau A, Vaccari A, et al. Functional aspects of meningeal lymphatics in ageing and Alzheimer's disease. Nature. 2018;560:185–91.
9. Weed LH. Studies on cerebro-spinal fluid. No. III: the pathways of escape from the subarachnoid spaces with particular reference to the arachnoid villi. J Med Res. 1914;31(1):51–91.
10. Andrew B, Xu M, Wang W, Hu J. The Paravascular Pathway for Brain Waste Clearance: Current Understanding, Significance and Controversy. Front Neuroanat. 2017;11:101.
11. Wardlaw JM, Benveniste H, Nedergaard M, et al. Perivascular spaces in the brain: anatomy, physiology and pathology. Nat Rev Neurol. 2020;16:137–53.
12. Aspelund A, Antila S, Proulx ST, et al. A dural lymphatic vascular system that drains brain interstitial fluid and macromolecules. J Exp Med. 2015;212(7):991–9.
13. Dong YQ, Stewart T, Bai LD, et al. Coniferaldehyde attenuates Alzheimer's pathology via activation of Nrf2 and its targets. Theranostics. 2020;10(1):179–200.
14. Bakker ENTP, Naessens DMP, VanBavel, Ed. Paravascular spaces: entry to or exit from the brain? Exp Physiol. 2019;104:1013–7.
15. Fultz NE, Bonmassar G, Setsompop K, et al. Coupled electrophysiological, hemodynamic, and cerebrospinal fluid oscillations in human sleep. Science. 2019;366(6465):628–31.
16. Frederickson CJ, Giblin LJ, Krezel A, et al. Concentrations of extracellular free zinc (pZn)(e) in the central nervous system of man, rat and rabbit during anesthesia, ischemia and reperfusion. Exp Neurol. 2006;198:285–93.
17. Zhang BB, Ren MQ, Sheu FS, Watt F, Routtenberg A. Quantitative analysis of zinc in rat hippocampal mossy fibers by nuclear microscopy. Neurosci Res. 2012;74(1):17–24.
18. Takeda A. Movement of zinc and its functional significance in the brain. Brain Res Rev. 2000;34(3):137–48.
19. Weiss JH, Sensi SL, Koh JY. Zn^{2+}: A novel ionic mediator of neural injury in brain disease. Trends Pharmacol Sci. 2000;21:395.

20. Frederickson CJ, Klitenick MA, Manton WI, Kirkpatrick JB. Cytoarchitectonic Distribution of Zinc in the Hippocampus of Man and the Rat. Brain Res. 1983;273(2):335–9.
21. Assaf SY, Chung SH. Release of Endogenous Zn^{2+} from Brain-Tissue during Activity. Nature. 1984;308(5961):734–6.
22. Saito H, Cherasse Y, Suzuki R, Mitarai M, Ueda F, Urade Y. Zinc-rich oysters as well as zinc-yeast- and astaxanthin-enriched food improved sleep efficiency and sleep onset in a randomized controlled trial of healthy individuals. Mol Nutr Food Res. 2017;61(5):1600882.
23. Ji XP, Liu JH. Associations between Blood Zinc Concentrations and Sleep Quality in Childhood: A Cohort Study. Nutrients. 2015;7(7):5684–96.
24. Cherasse Y, Urade Y. Dietary Zinc Acts as a Sleep Modulator. Int J Mol Sci. 2017;18(11):2334.
25. Xiao RY, Yuan L, He WJ, Yang XD. Zinc ions regulate opening of tight junction favouring efflux of macromolecules via the GSK3 beta/snail-mediated pathway. Metallomics. 2018;10(1):169–79.
26. Xu ZH, Zhang CY, Zhang Y, Yang XD. Europium Complexes as Novel Indicators of Paracellular Diffusion. Chem Biodivers. 2012;9(9):1916–22.
27. Qian F, Zhang CL, Zhang YM, et al. Visible Light Excitable Zn^{2+} Fluorescent Sensor Derived from an Intramolecular Charge Transfer Fluorophore and Its in Vitro and in Vivo Application. J Am Chem Soc. 2009;131(4):1460–8.
28. Roher AE, Kuo YM, Esh C, et al. Cortical and leptomeningeal cerebrovascular amyloid and white matter pathology in Alzheimer's disease. Mol Med. 2003;9:112–22.
29. Keable A, Fenna K, Yuen HM, et al. Deposition of amyloid beta in the walls of human leptomeningeal arteries in relation to perivascular drainage pathways in cerebral amyloid angiopathy. Biochim Biophys Acta. 2016;1862:1037–46.
30. Herzig MC, Winkler DT, Bürki K, et al. Aβ is targeted to the vasculature in a mouse model of hereditary cerebral hemorrhage with amyloidosis. Nat neurosci. 2004;7:954–60.
31. Salinas JD, Saporito-Irwin SM, Cotman CW, Nostrand WEV. Amyloid β-Protein Induces Its Own Production in Cultured Degenerating Cerebrovascular Smooth Muscle Cells. J Neurochem. 1995;65(2):931–4.
32. Clifford PM, Siu G, Kosciuk M, et al. α7 nicotinic acetylcholine receptor expression by vascular smooth muscle cells facilitates the deposition of Aβ peptides and promotes cerebrovascular amyloid angiopathy. Brain Res. 2008;1234(1):158–71.
33. Hampshire A, Trender W, Chamberlain SR, et al. Cognitive deficits in people who have recovered from COVID-19. EClinicalMedicine. 2021;00:101044.
34. Zhou YD, Xu JL, Hou Y, et al. Network medicine links SARS-CoV-2/COVID-19 infection to brain microvascular injury and neuroinflammation in dementia-like cognitive impairment. Alzheimer Res Ther. 2021;13(1):110.
35. Nuovo GJ, Magro C, Shaffer T, et al. Endothelial cell damage is the central part of COVID-19 and a mouse model induced by injection of the S1 subunit of the spike protein. ANN Diagn Pathol.

2021;51:151682.

Figures

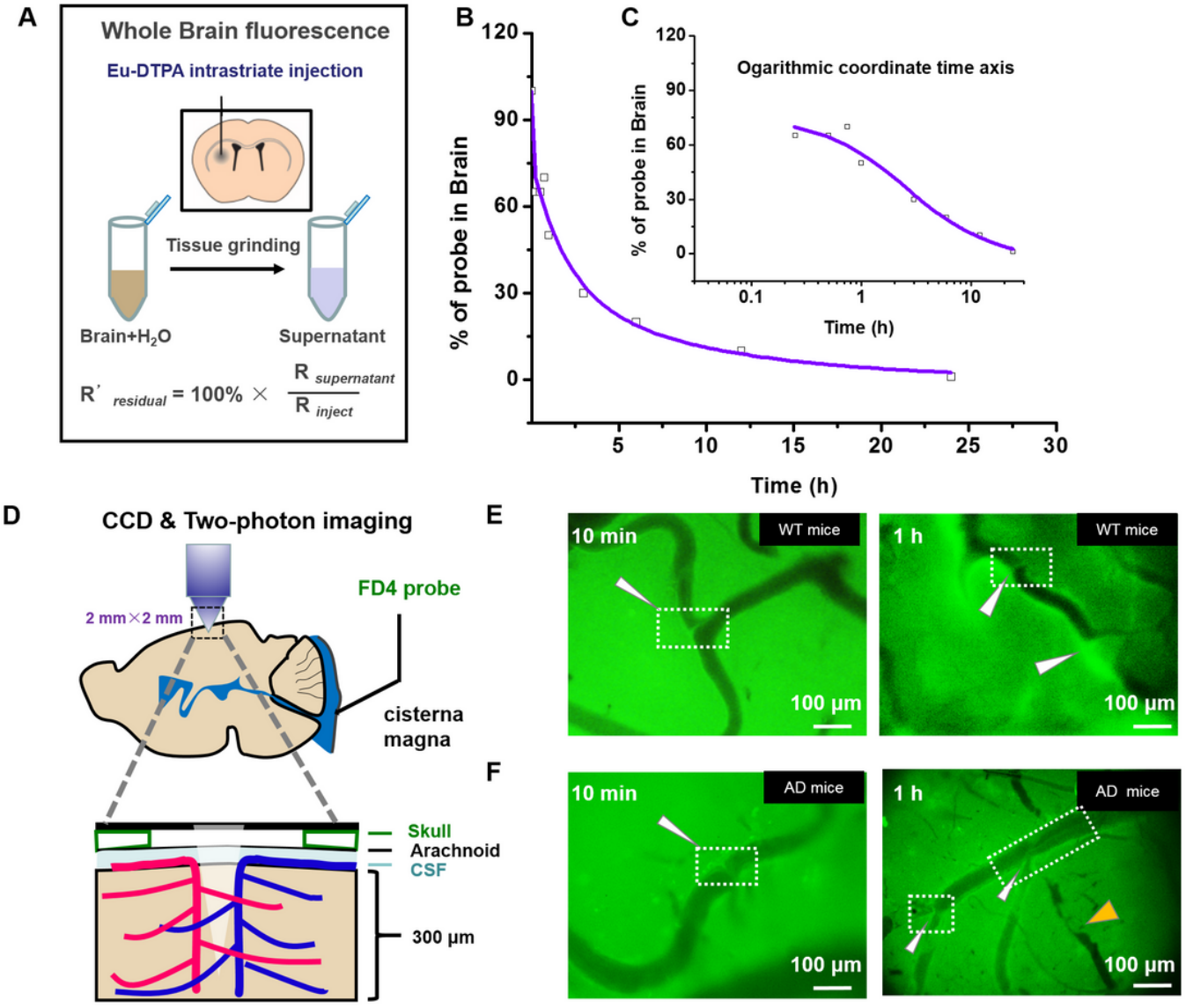

Figure 1

The rapid drainage of brain CSF-ISF tracer is through pore path on venule wall. (A) small molecular BBB-impermeable tracer, Eu-DTPA complexes, was injected into the mouse striatum and the clearance from the brain parenchyma was evaluated as described in Materials and Methods. (B) The time process of drainage of intrastriate Eu-DTPA probe. The process of drainage of Eu-DTPA with logarithmic coordinate time axis. C57BL/6 mice (n=5) were intrastriate injected with Eu-DTPA probe. Then, 5 min, 15 min, 0.5 h, 1 h, 3 h, 6 h, 12 h, and 24 h after the administration, animals were immediately decapitated and the brain was harvested. Then, the residual Eu content was measured by time-resolved fluorescence. Data was

fitted to a triple phasic decay model using an Origin 8.0 program. (C) Illustration of experimental imaging setup of in vivo observation of the dynamics of paravascular CSF tracers (fluorescein isothiocyanate–dextran-4 (FD4): molecular size, 4 kD) flux into the mouse cortex and blood vessel. Imaging was conducted between 0 and 300 μm below the cortical surface. (D, E) Dynamic CSF fluorescence imaging in healthy WT mice (D) and AD model mice (E) (APPswe/PS1dE9 (APP/PS1) transgenic mice) with FD4 tracer injected into the mouse cisterna magna. White arrow indicates the spots for CSF entering the lumen of the blood vessel. Yellow arrow indicates the lumen of the blood vessel with stacking CSF fluorescent tracers. Scale bars, 100 μm [(D) and (E)].

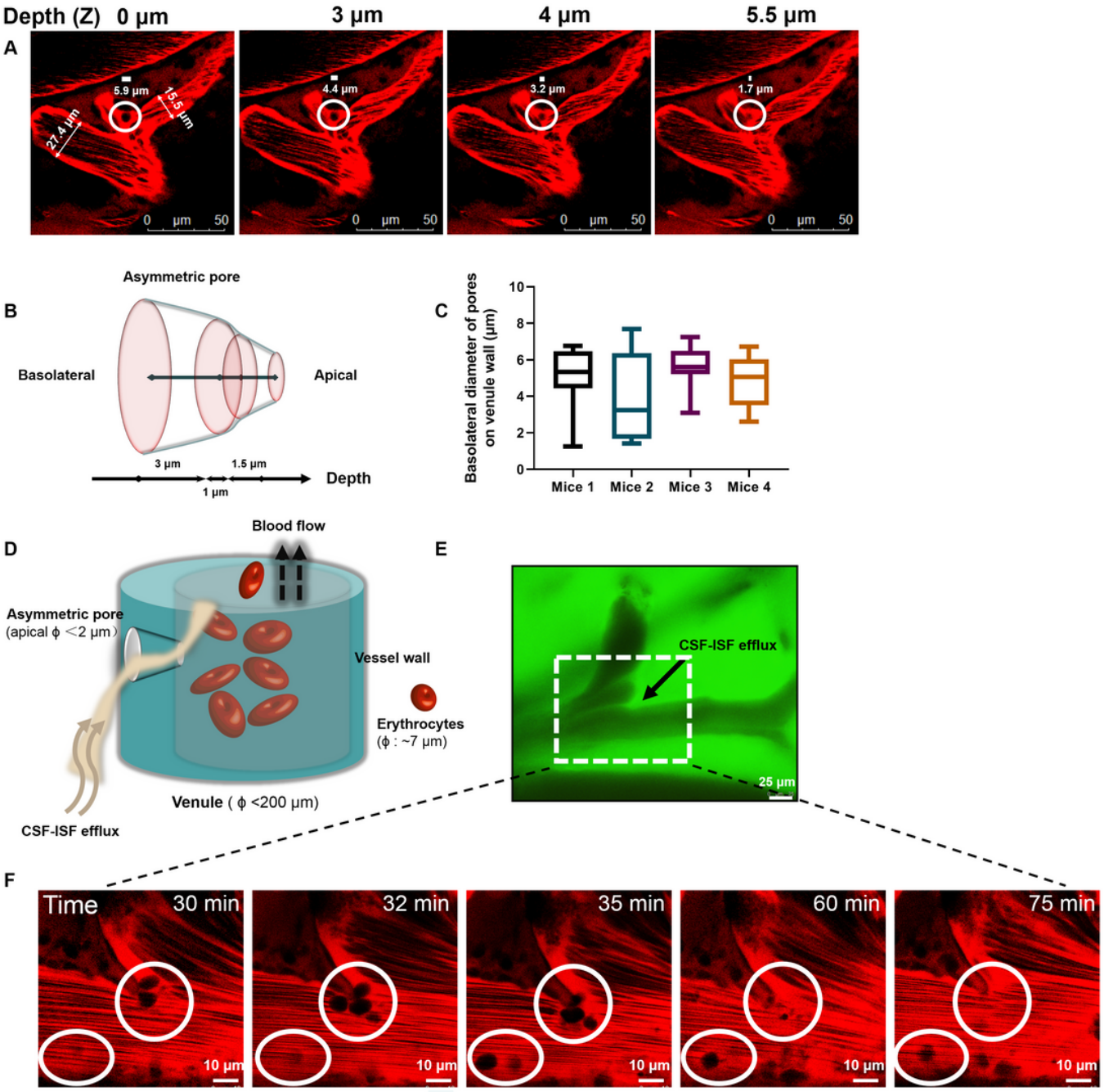

Figure 2

The dynamic asymmetric trumpet-like pores on venule mediate direct entry of subarachnoid CSF-ISF into blood vessels. The cerebral vasculature was visualized by intravenously injected TRITC70 (Tetramethylrhodamine–dextran-70 (TRITC70): molecular size, 70 kD), and identified morphologically using two-photon and CCD dynamic imaging. (A) The pores on venule were observed at the site for CSF tracer entering the brain blood vessels from paravenous spaces. The four images were light section on a typical pore at 3, 1, 1.5-μm intervals on a venule located between 0 and 300 μm below the cortical surface. The diameter along the depth from the basolateral to apical was 5.9, 4.4, 3.2 and 1.7-μm, respectively. (B) Schematic of the shape of the asymmetric trumpet-like pore on venule observed in (A). (C) Quantification of the basolateral diameter of pores on venule wall in the 2 mm×2 mm cranial window in four wild type (WT) mice. (D, E) Dynamic CSF fluorescence imaging in WT mice with FD4 tracer injected into the mouse cisterna magna (D). White rectangle and black arrow indicate the spots for CSF entering the lumen of the blood vessel as well as the position that two-photon imaging conducted in (E). (E) The vessel images conducted from 30, 32, 35, 60, 75 min after the CSF tracer injected. Cycles indicate the dynamic change of the pores on venule wall. (F) Schematic depiction of CSF-ISF flux through the asymmetric channel when moving along the paravenous space. Scale bars, 50 μm (A), 25 μm (D), and 10 μm (E).

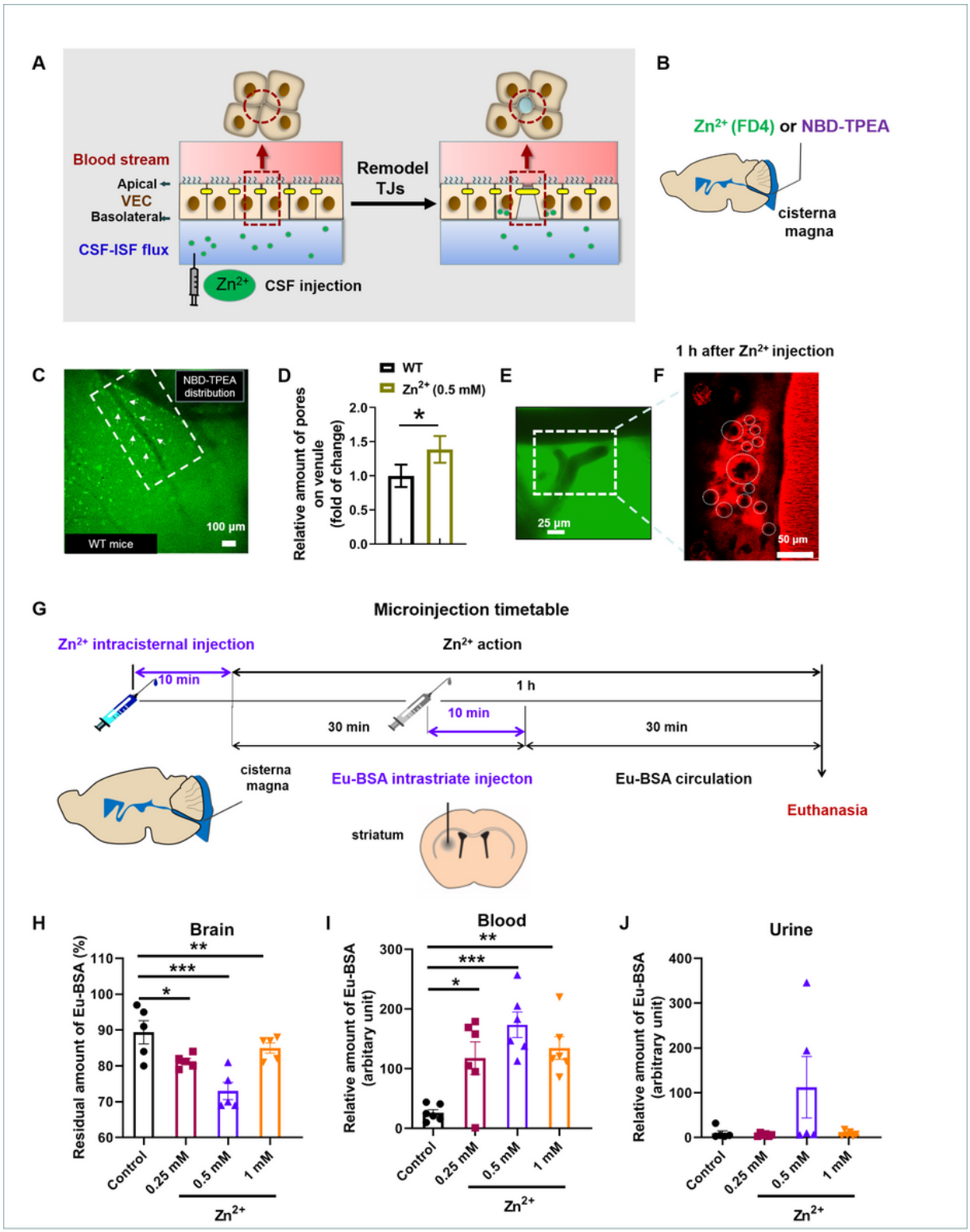

Figure 3

Zn2+ enhanced the interstitial solute and fluid clearance from the brain potentially by promoting pore formation via inducing the TJs remodeling in vascular endothelial cells (VECs). (A) Schematic of potential mechanism for formation of the asymmetric trumpet-like pores on venule. Zn2+ was injected into the subarachnoid CSF and assumed to collect in paravenous space to exert influence on VECs from the basolateral side to induce TJs remodeling. (B) Illustration of the movement of ventricular and

subarachnoid Zn2+ (together with FD4) or Zn2+ probe (NBD-TPEA) into the brain parenchyma. (C) visualization of Zn2+ after 30 min of intraventricular infusion with NBD-TPEA fluorescence probe. (D) In around one hour after intracisternal injection of Zn2+ (0.5 mM), the relative amount of dynamic pores on venule was significantly increased (*p < 0.05, n = 4) compared to WT controls. (E, F) A typical view of pores on venule on dynamic CSF fluorescence image (E) and two-photon imaging (F). The effects of Zn2+ on the clearance of macromolecules were verified (G-J). (G) Illustration injection design of Eu-BSA (striatum injection) and Zn2+ (intracisternal injection). The volume of all injection was 2 μl. (H) The relative brain Eu-BSA content upon treatment with Zn2+ (0.25 mM, 0.5 mM, 1 mM). (I, J) The relative amounts of Eu-BSA in peripheral blood (I) and urine (J). Data represented as mean ± SEM (n=5–6). ***p<0.001, **p<0.01, *p<0.05 versus untreated control mice. Scale bars, 100 μm (C), 25 μm (E), and 50 μm (F).

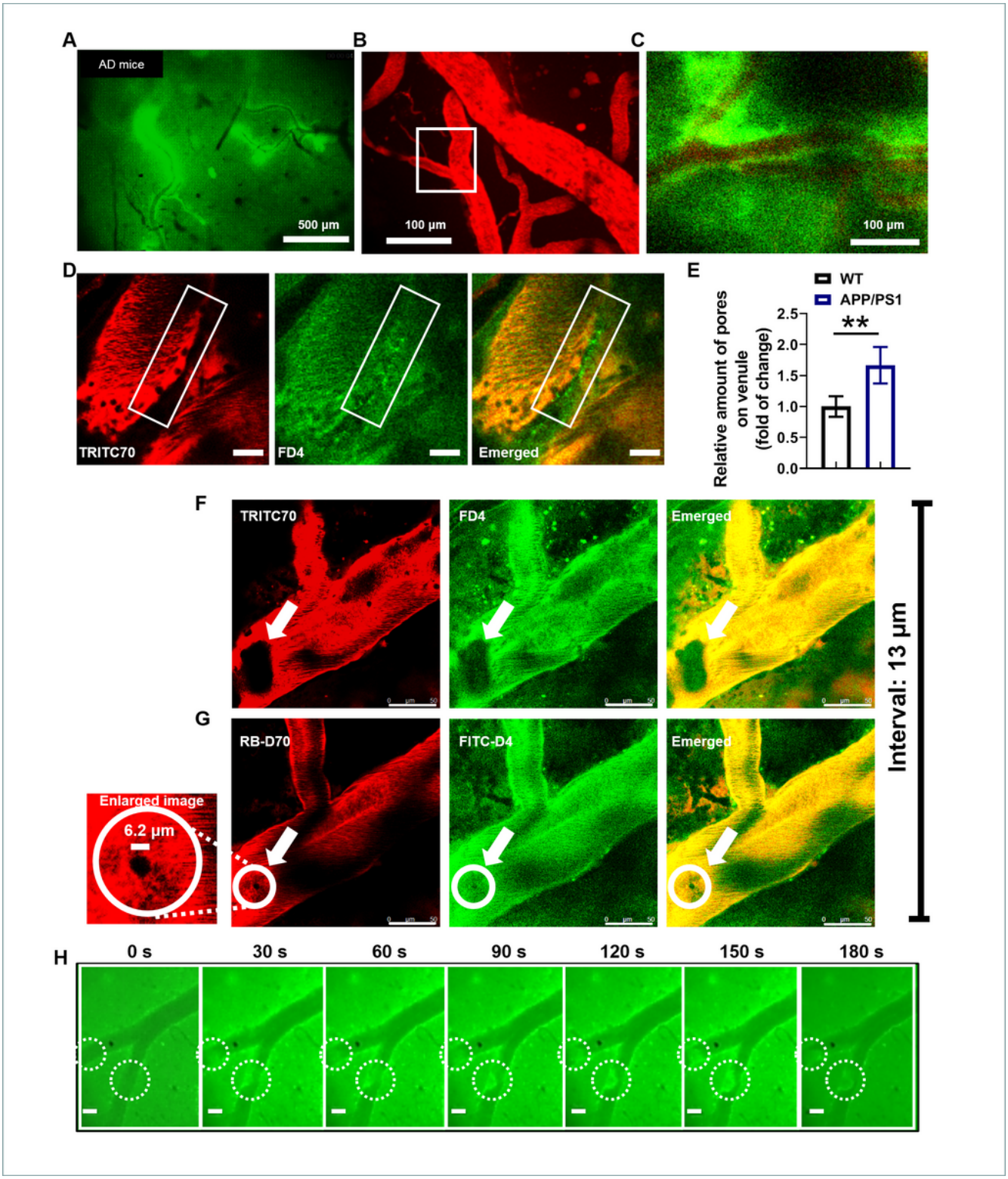

Figure 4

The impacts of heavy Aβ burden on the pore path formation and Aβ clearance in AD model mice. (A-D) Distribution of CSF fluorescence tracer (FD4) after around one hour of intracisternal infusion in AD model mice. (A) Accumulation of FD4 fluorescent tracers in the perivascular space of multiple blood vessels in AD model mice. (B) The cerebral vasculature visualized by intravenously injected TRITC70 (Red) and (C) the influx of FD4 (green) around vasculature. (D, E) A pore on venule was visualized underneath the

sheathed of the CSF tracer at 13 μm above the pore. White arrows depict the CSF tracer sheathed (D) and the pore (E). (F) The relative amount of dynamic pores on venule in AD mice was significantly increased compared to WT controls (**p < 0.01, n = 4) (G) The two-photon image of the pores and the CSF tracers surround. (H) Dynamic CSF fluorescence imaging in AD mice with FD4 tracer injected into the mouse cisterna magna. Arrows indicate the spots for CSF squeezed into drainage veins from the perivenous space at 30 s intervals. Scale bars, 500 μm (A), 100 μm [(B) and (C)], 50 μm [(D) and (E)], 25 μm (G), and 100 μm (H).

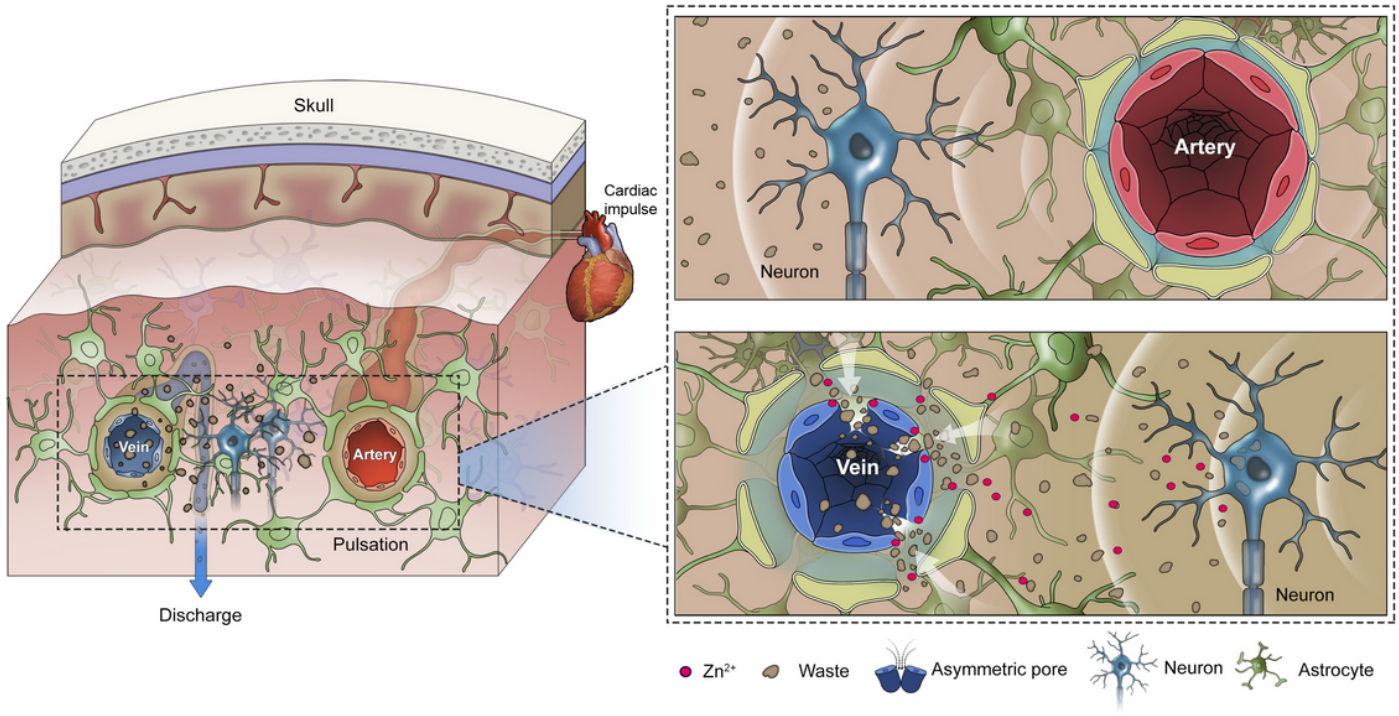

Figure 5

Schematic depiction of conjectured routes through dynamic asymmetric pores on venule and the potential mechanism. In this brain-wide pathway, CSF enters the brain along para-arterial routes [1-5], convective bulk ISF flow drives the clearance of interstitial solutes and fluid from the brain parenchyma to paravenous routes. Meanwhile, the TJs of VECs were remodeled to form dynamic asymmetric pores by some regulatory mechanism such as zinc ions, then solutes and fluid can enter the bloodstream across the pores on venule to complete the whole brain drainage.

Supplementary Files

This is a list of supplementary files associated with this preprint. Click to download.

- MolecularDegenerationSupplementarymaterials.docx
- MovieS1.mp4
- MovieS2.mp4

- MovieS3.mp4
- MovieS4.mp4
- MovieS5.mp4
- MovieS6.mp4
- MovieS7.mp4
- MovieS8.mp4